UNIVERSITATEA BABEȘ-BOLYAI, **Facultatea de Fizică**, Cluj-Napoca

Dysprosium and iron based contrast agents for Nuclear Magnetic Resonance Imaging - synthesis and characterization

Ph.D. THESIS SUMMARY

Ph.D. student,
Liviu Chiriac

Promoter,
Prof.dr. Simion Simon

Cluj-Napoca 2019

Contents

Key-words: ***Contrast agents; Nuclear Magnetic Resonance Imaging; Theranostic; Dysprosium; Iron, Biocompatibility.***

Aim of the thesis

In recent decades, lot of scientific research work was focused on developing diagnostic and treatment techniques in the medical field, particularly with regard to cancer therapy. Nuclear Magnetic Resonance Imaging (MRI) is primarily used to diagnose a variety of afflictions, encompassing tumors and demyelinating diseases in the brain, fine meniscal lesions, arteries and veins injuries [1-5]. When using MRI contrast agents, it has developed the idea of obtaining materials which, in addition to properties of magnetic resonance contrast agent, also have properties for targeted treatments [6]. These are named theranostic materials [7]. Contrast agents used in MRI are classified according to their influence on the relaxation times in three major groups: positive contrast agents which shorten the spin-lattice T_1 relaxation time - their distribution will produce images with increased signal intensity / hypersignal areas (bright areas); contrast agents that affect spin-spin relaxation time T_2 (negative contrast agents) - their presence will induce hyposignal areas (dark areas) and dual contrast agents - they affect in equal weight and spin-lattice relaxation time and spin-spin relaxation time [8].

The purpose of this thesis was to investigate potential novel contrast agents, based on dysprosium and iron, for the MRI investigation method, and which could also be considered for their use in hyperthermia treatments.

Samples preparation and the related investigations were carried out at the Institute of Interdisciplinary Research in Bio-Nano-Sciences and at the National Magnetic Resonance Center at the Faculty of Physics of "Babeş-Bolyai" University of Cluj-Napoca.

The sol-gel method primarily used in the preparation of the samples studied in the thesis is widely applied to obtain a large range of new materials, with applications several fields, both technological and biomedical. The sol-gel process allows the synthesis of oxide materials with desirable properties regarding hardness, optical transparency, chemical durability and thermal resistance, their structure being typically acieved at room temperature, unlike conventional melt cooling techniques, which involve much higher temperatures [9, 10]. Applying the sol-gel method, materials can be obtained in a wide variety of applications: ultrafine powder, thin films, fibers, microporous membranes, and highly porous materials. Also, starting from the sol-gel method powder samples can be obtained by freeze-drying or spray-drying by freeze-drying or spray-drying.

Experimental results for dysprosium containing system

Samples of $xDy_2O_3 \cdot (100-x)SiO_2$ composition (x = 0, 5 and 10 mol %) were prepared by freeze drying (FD) and spay drying (SD) methods, starting from aqueous solutions of $Dy(NO_3)_3 \cdot 9H_2O$ and $Si(OC_2H_5)_4$ (TEOS) of analytical reagent grade purity. The samples notation further used in this work is x-FD and x-SD based on their composition (xDy_2O_3) and drying method. The synthesis was carried out by hydrolysis and polycondensation of stoichiometric amounts of oxide precursors. The hydrolysis reaction of TEOS was acid catalysed with HCl added dropwise until the pH was close to 3.0, under stirring at room temperature for about 60 min. Thereafter the mixed solutions were vigorously stirred for about 1h at 50 ^{o} C. The resulting sols were divided into two equal parts further subjected to two methods for extracting the solvent, i.e., (*i*) freeze drying and (*ii*) spray drying. In the first case (*i*) the sol was stirred until gelation and then the gel was quickly frozen in liquid nitrogen for 15 minutes. The frozen gel was lyophilized for 2 weeks at a temperature ranging from -50^{o}C to -54 ^{o} C, with vacuum pressure in the range 0.04-0.024 mbar. The samples were lyophilized using an Alpha 1-2 LD Christ Freeze Dryer. In the second case (*ii*) the sol was spray dried at inlet temperature of 110 ^{o}C and outlet temperature between 67 and 69 ^{o}C using a Buchi-290 Mini Spray-dryer with two-fluid nozzle. Spray nozzle had a nozzle tip of 5 mm. The flow type was co-current with mixing of air and liquid/sol at the nozzle head. The air spray flow rate was 45 l/h and the aspirator rate was kept constant at 93%. Based on thermal analysis results [11], the samples were heat treated at 600^{o}C .

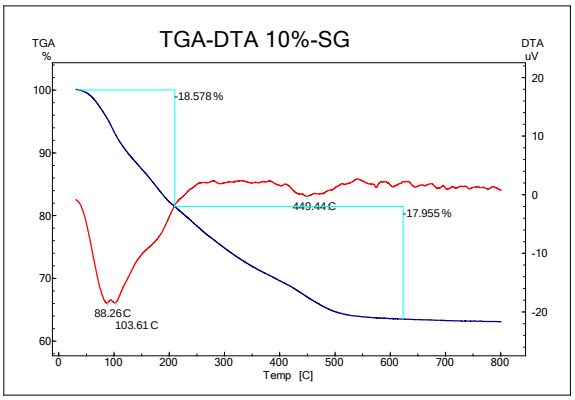

DTA and TGA traces for 10% Dy_2O_3 –SG sample

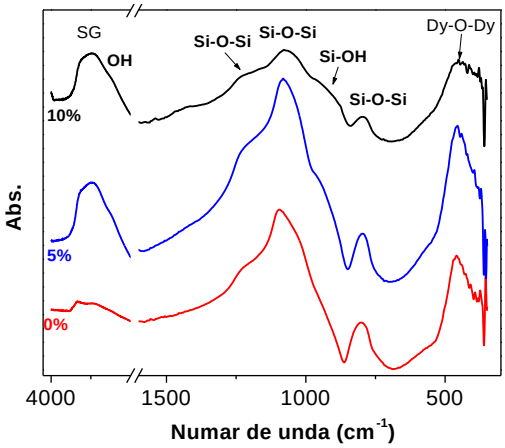

FT-IR spectra for heat treated SG samples

X- ray results point out the amorphous state al all SG, FD and SD samples both before and after 600^{o}C heat treatment. Similar results are delivered by the infrared spectroscopic analysis following the absorption bands arising from Si–O–Si and Dy-O-Dy vibrations.

Particle size and zeta potential were measured by the dynamic light scattering method. According to these measurements, the mean particle size is between 0.5 and 4 μm, the negative

zeta potential, between -16 and -44 mV, that indicates good stability of the suspensions obtained with the studied samples.

The XPS analysis carried out on the outermost layer of the investigated samples evidences the occurrence of dysprosium on their surface proportionally to Dy_2O_3 amount introduced in silica host matrix. The peak area ratios normalized by the atomic sensitivity factors indicates a higher content of Si and a lower value for O content compared to the theoretical composition.

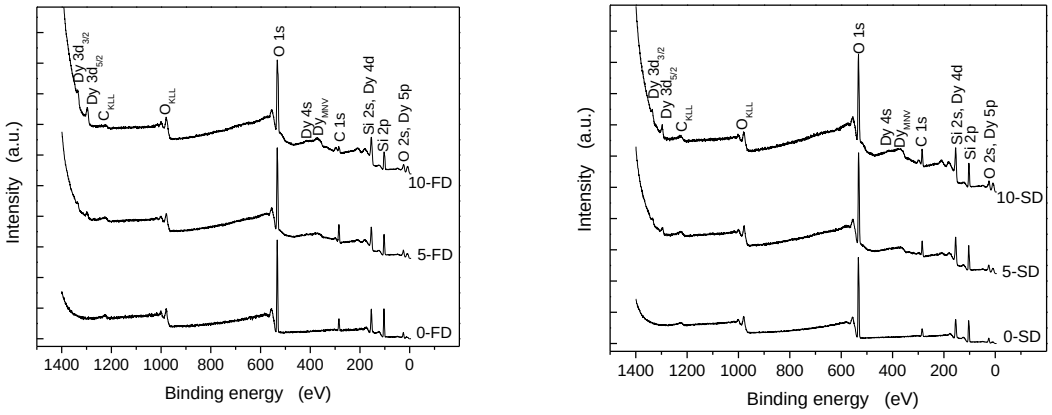

(a) *(b)*

XPS survey spectra for (a) FD and (b) SD samples

The oxygen depletion could suggest surface defects associated with oxygen vacancies. Concerning the Dy/Si ratio on the surface it is clearly seen that this ratio is quite close to the theoretical bulk value. The presence of carbon is due to the ubiquitous carbon contamination of all samples exposed to the atmosphere.

Expected elemental composition (at %) in $xDy_2O_3 \cdot (100-x)SiO_2$ of homogeneous assumed samples and the elemental composition on the outermost layer of samples experimentally determined by XPS with carbon omission.

Element / x (mol%)		O	Si	Dy	Dy/Si
theoretical	**0**	66.7	33.3	-	-
	5	66.2	30.6	3.2	0.10
	10	65.6	28.1	6.3	0.22
experimental	**0-FD**	53.3	46.7	-	-
	5-FD	55.3	41.2	3.5	0.08
	10-FD	55.5	38.1	6.4	0.17
	0-SD	53.9	46.1	-	-
	5-SD	54.1	42.0	3.9	0.09
	10-SD	53.0	39.7	7.3	0.18

In order to investigate the atomic environments on the surface of the particles the O 1s and Si 2p XPS core level spectra were further investigated. High resolution O 1s spectra are recorded in the range 525-540 eV.

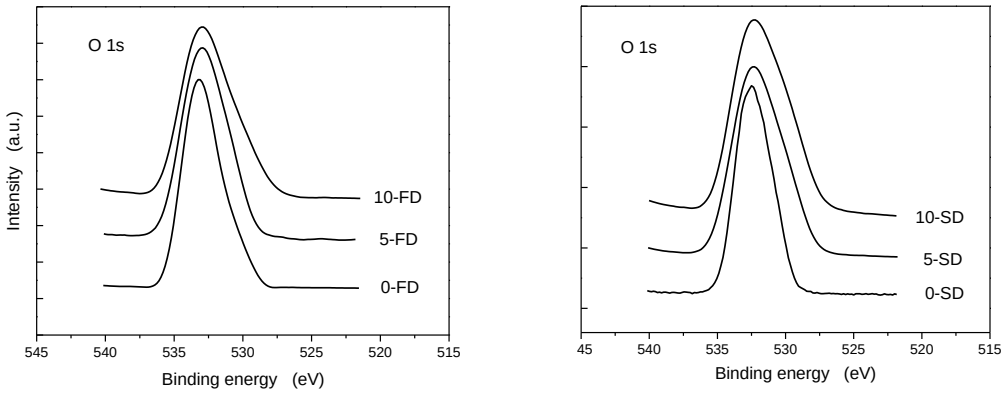

(a) (b)

XPS O 1s core level spectra of (a) FD and (b) SD samples

The NBO/BO ratio of non-bridging oxygens (NBO) and bridging oxygens (BO), was determined in a first attempt by including all contributions of non-NBO oxygen in a single component. A rough decomposition of these spectra with two components around 533 and 531 eV, assigned to bridging and non-bridging oxygens, respectively, was carried out using Voigt (Gaussian-Lorentzian mixed) line shape. The results show that the ratio of non-bridging to bridging oxygens (NBO/BO) on samples surface depend both on composition and preparation method. The BO component is assigned to Q^4 units while NBO component include contributions from oxygens involved in Q^n units with $n<4$. More components for non-bridging oxygens would improve the fit but the first attempt was to include all NBO contributions in a sole component to evaluate the NBO/BO ratio.

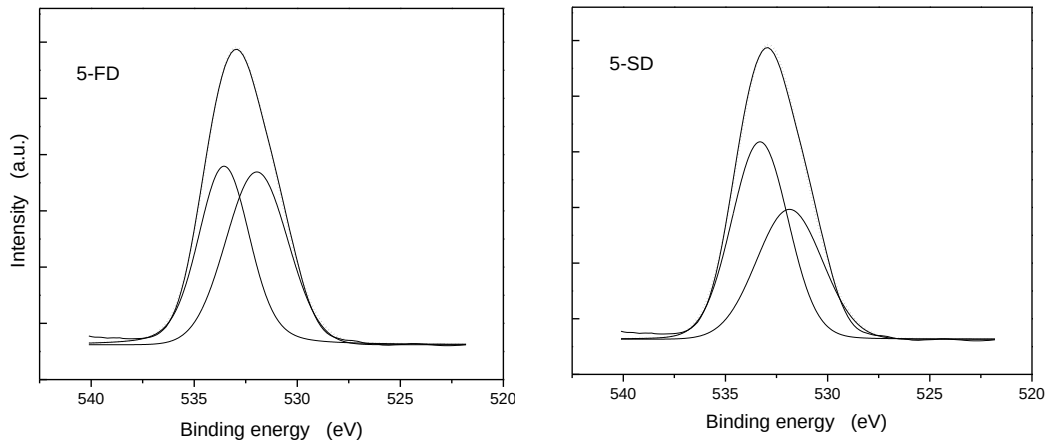

(a) *(b)*

Deconvolution of XPS O 1s core level spectra of (a) FD and (b) SD samples in BO and NBO components

The analysis of Si 2p XPS core level spectra points out that the binding energy of Si 2p photoelectrons is close to 103 eV. The value reported for pure SiO_2 glass is 103.6 eV. A slight shift to lower binding energy is observed by Dy_2O_3 addition.

By increasing the concentration of Dy_2O_3 the structural changes induced at the local structure in the samples are also evidenced by the modification of ^{29}Si NMR spectra. The ^{29}Si MAS-NMR spectra of the lyophilized samples before thermal treatment have broad lines ranging from 80-130 ppm.

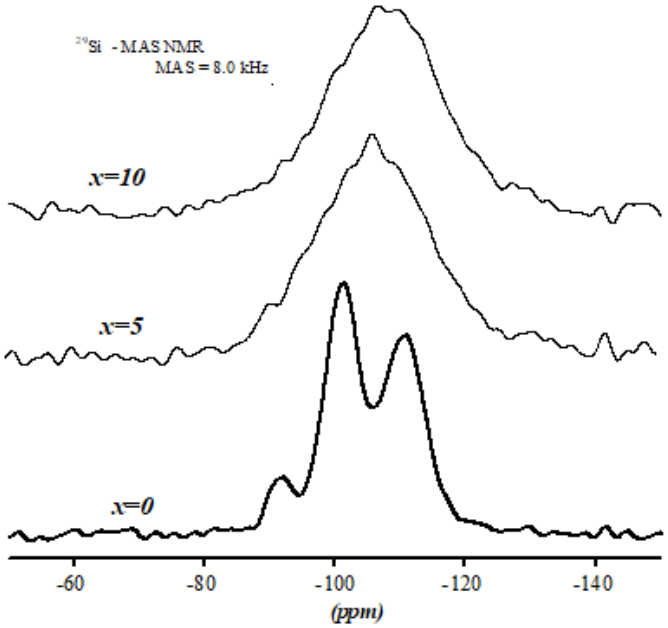

^{29}Si MAS RMN spectra of as-prepared FD samples

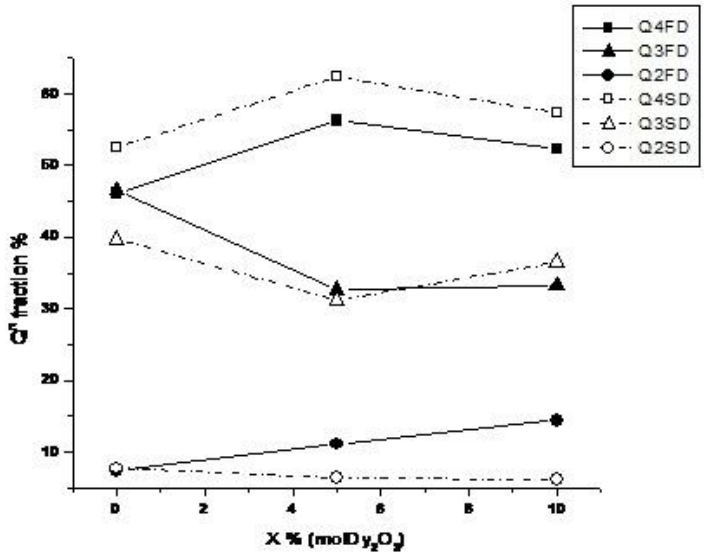

Dependence of Q^n fraction (%) on the composition of as-prepared FD and FD samples

The analysis of ^{29}Si MAS-NMR spectra FD samples shows the changes in the polymerisation of the silicate matrix caused by Dy_2O_3 addition. For SD samples, the analysis of ^{29}Si MAS-NMR spectra based on spectra deconvolution data denotes a similar dependence of Q^n. The Q^n fractions both for FD and SD samples with 5 % and 10% Dy_2O_3 content are relatively close indicating a similar silica network. But on the other hand, the composition dependence of Q^n structural units for FD and SD samples show a higher interconnection of the structural units in the samples obtained by freeze drying as compared with that obtained by spray drying. On the other hand, due to the presence of paramagnetic Dy^{3+} ions nearby some silicium atoms, the relaxation time of their nucleus is dramatically changed.

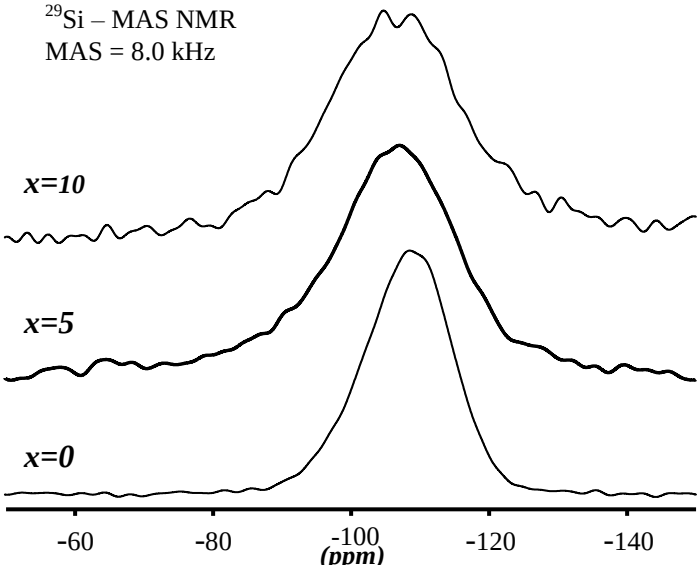

^{29}Si MAS RMN spectra of heat-treated FD samples

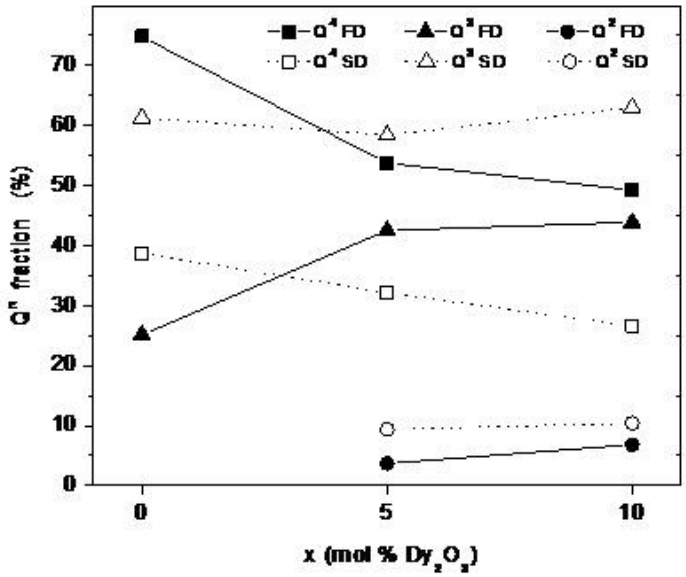

Dependence of Q^n fraction (%) on the composition of heat-treated FD and FD samples

The analysis of ^{29}Si MAS-NMR spectra FD samples shows the changes in the polymerisation of the silicate matrix caused by Dy_2O_3 addition.

The deconvolution data for (100-x)SiO_2·xDy_2O_3 as-prepared FD samples

Sample	$Q^{(n)}$	Chemical shift (ppm)	Line width (ppm)	$Q^{(n)}$ fraction (%)
100(SiO_2)	Q^2	-91.93	4.69	5.34
	Q^3	-101.11	6.29	46.53
	Q^4	-110.59	5.58	46.13
95(SiO_2) 5(Dy_2O_3	Q^2	-90.50	15.88	11.05
	Q^3	-103.25	15.05	32.64
	Q^4	-111.00	16.99	56.29
90(SiO_2) 10(Dy_2O_3)	Q^2	-91.95	4.94	1.59
	Q^3	-101.46	14.66	34.31
	Q^4	-109.41	16.60	64.10

The deconvolution data for (100-x)SiO_2·xDy_2O_3 heat-treated FD samples

Sample	$Q^{(n)}$	Chemical shift (ppm)	Line width (ppm)	$Q^{(n)}$ fraction (%)
100(SiO_2)	Q^2	-	-	-
	Q^3	-102.00	15.53	25.15
	Q^4	-109.55	13.06	54.83
95(SiO_2) 5(Dy_2O_3)	Q^2	-93.21	5.50	3.51
	Q^3	-102.35	15.00	42.53
	Q^4	-111.49	18.06	53.56
90(SiO_2) 10(Dy_2O_3)	Q^2	-91.92	8.33	1.59
	Q^3	-102.00	19.11	36.90
	Q^4	-110.98	24.58	61.31

The results obtained from the deconvolutions performed on the spectra recorded on both types of samples, FD and SD, show that for 5% and 10% Dy_2O_3 the ratio of Qn units is relatively similar indicating a similar silica matrix for the two synthesis methods.

In order to evaluate the contrast enhancement capacity in nuclear magnetic resonance imaging, namely for the characterization of T_1 and T_2 parameter evolution for the compounds of the three systems, RARE-T1 and RARE-T2 protocols were investigated (RARE - rapid acquisition with relaxation enhancement pulse sequence / fast acquisition refocused echo).

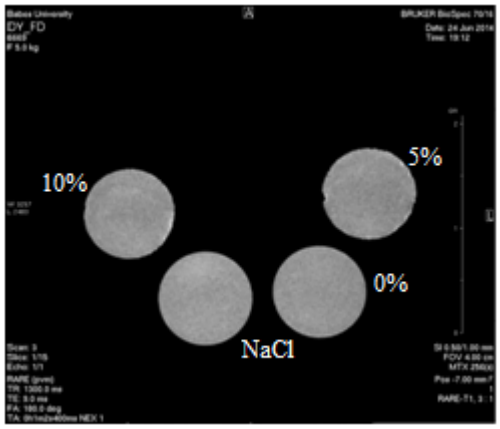

T_1-weighted images for FD samples acquired using Turbo RARE protocol

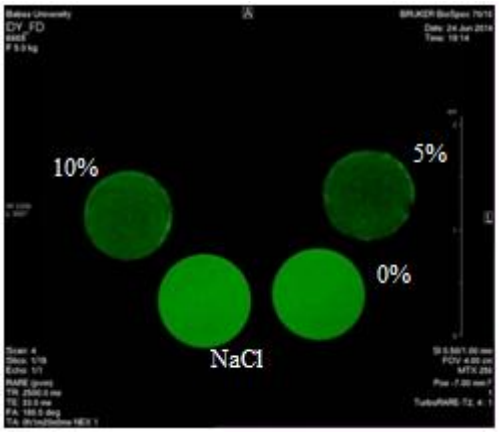

T_2-weighted images for FD samples acquired using Turbo RARE protocol

The T_2 relaxation time is influenced by local magnetic field fluctuations caused by the presence of magnetic centers, and local interaction. As can be seen in the above images, obtained with structural acquisition MRI protocol, the contrast synthesized contrast agent exhibits contrast characteristics due to relaxation time T_2, which is also confirmed by the relaxometry calculations. The results indicate that the T_2 relaxation time is clearly influenced by samples composition and structure. The best contrast is observed for samples with 5% mol Dy_2O_3.

For quantitative verification, relaxometry analyzes were performed with the RARE-T_1 + T_2-map protocol, which allows calculation of relaxation times for each echo time (ET) of the pulse sequence. TE is the time between the application of the radiofrequency excitation pulse and the moment at which the signal is measured. The relaxation time T_2 was measured from the intensity of the MRI signal at different TE values.

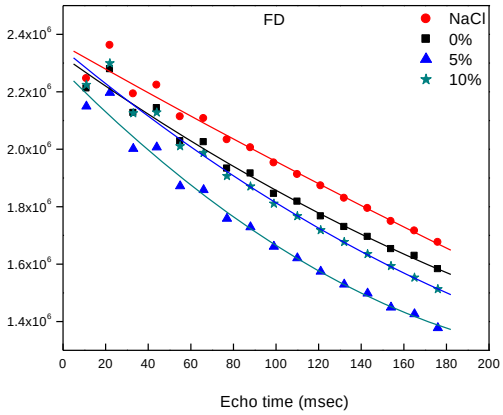

MRI signal intensity, in a.u., measured at different echo times, for FD samples

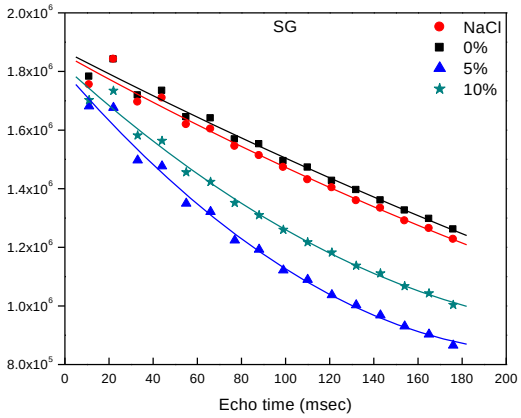

MRI signal intensity, in a.u., measured at different echo times, for SG samples

From the relaxometry data one notices the evolution of T_2, which is influenced by the particle size (in this case, nano- and micrometer scale), the Dy_2O_3 concentration and the fraction of Q_2, Q_3, Q_4 units. For FD samples with 5 and 10% Dy_2O_3, a lower T_2 relaxation time was determined than that obtained for the NaCl solution or for the sample without Dy_2O_3. For the sample with 5% Dy_2O_3, due to the fact that the particles are of nanometric size, a larger amount of sample will remain in the suspension, which is reflected in the low relaxation time, that results in an increased contrast.

In case of SD method, the lowest T_2 relaxation time was obtained for dysprosium free sample, while 5 and 10% Dy_2O_3 samples T_2 values were higher, indicating that due to the micrometric dimension of the particles, they did not remain in the suspension.

The samples were immersed in SBF and stored for 26 days at 37 °C, after which the MRI signals were reanalyzed using the relaxometric characterization protocol. Solutions in which the samples were immersed deliver a lower signal, because the dysprosium compounds are negative contrast agents. It is noted that the lowest value of the signal is given by 5% Dy_2O_3 samples.

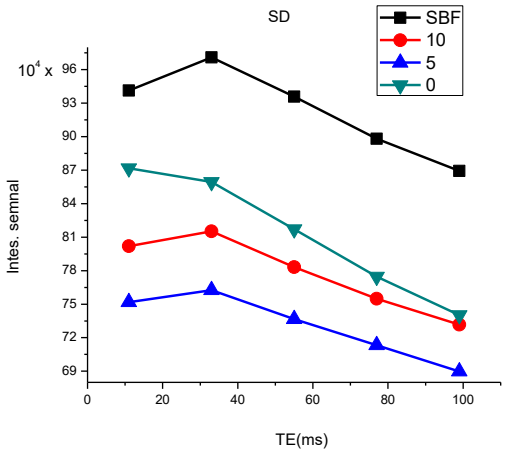

MRI signal intensity, in a.u., measured at different echo times, for SD samples after immersion in SBF

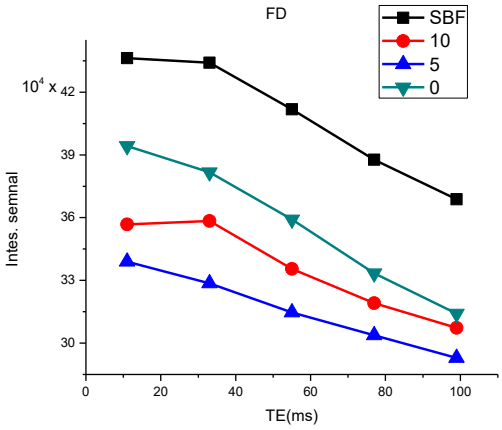

MRI signal intensity, in a.u., measured at different echo times, for FD samples after immersion in SBF

The most diminished signal intensity is obtained for FD sample with 5% Dy_2O_3, which is favorable because it is desired to introduce in the body an as low as possible amount of compounds belonging to the class of the rare earths. The results of these investigations motivated the further investigation of 5% Dy_2O_3 FD sample, namely toxicological tests on cell culture, and the ultimate goal is targeted to *in-vivo* investigations.

The biocompatibility tests were conducted at the University of Medicine and Pharmacy, Cluj-Napoca, on umbilical cord-specific HUVEC cells and on DLD1 colon cancer-specific cells. The tests were repeated 3 times for an accurate analysis. For 5% Dy_2O_3 FD sample, it can be seen from the HUVEC test set that only 100000 µg / ml appears harmful. For 5% Dy_2O_3 SD samples

for all dilutions is evidenced biocompatibility with the cells, and for samples with 10% Dy_2O_3, only a high concentration of 100000 μg / ml of the sample is of high toxicity.

The tests on colon carcinogenic DLD1 cells showed that only the dilution with 100000 μg / ml destroys the cells.

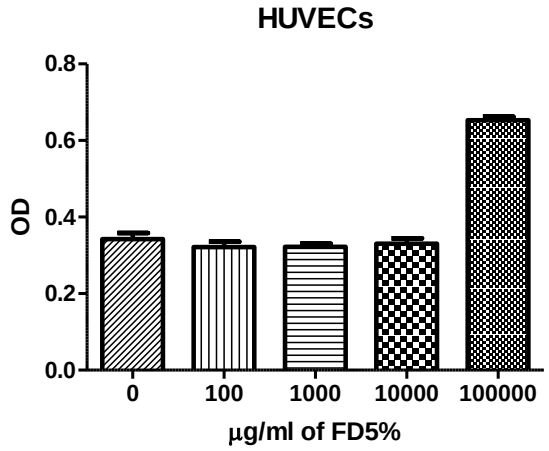

0 vs 100000	Yes	***
0 vs 10000	No	ns
0 vs 1000	No	ns
0 vs 100	No	ns

Testele pe celule HUVEC cu diluţii între 100 şi 100000 μg/ml de probă FD 5% Dy_2O_3

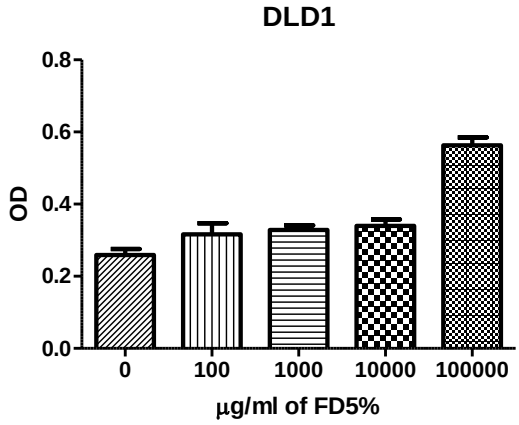

0 vs 100000	Yes	***
0 vs 10000	Yes	**
0 vs 1000	Yes	**
0 vs 100	Yes	*

Testele pe celule DLD1cu diluţii între 100 şi 100000 μg/ml de probă FD 5% Dy_2O_3

Experimental results for iron containing system

Sol-gel derived particles with nominal composition $(100-x)[0.7SiO_2 \cdot 0.3Na_2O] \cdot xFe_2O_3$, with $0 \leq x \leq 20$ mol%, were prepared by sol-gel method. The samples were prepared starting from analytical purity grade solutions of tetraethoxysilane ($Si(OC_2H_5)_4$ - TEOS), sodium nitrate ($NaNO_3$) and iron nitrate $Fe(NO_3)_3$. The sols were devided in two parts differently dried: *(i)* by classical sol-gel method (noted SG) / after gelation the gels were dried at 35 ^oC, and *(ii)* by freeze dryeng (noted FD) / lyophilization.

Based on thermal analysis results [12] the samples were heat treated at 600^oC for 3 hours.

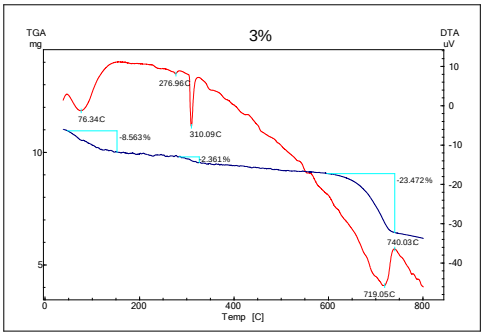

DTA and TGA runs for x=3%

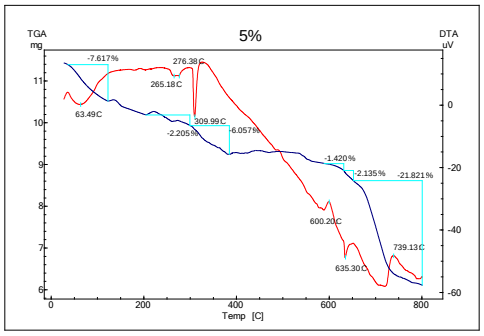

DTA and TGA runs for x=5%

In X-ray diffractograms, narrow and intense lines specific to nitrate crystals are identified, denoting undissolved residues of the nitrates used as Fe_2O_3 and Na_2O precursors.

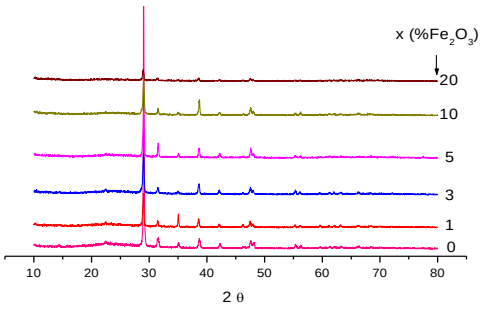

DRX patterns of as-prepared FD iron containing samples

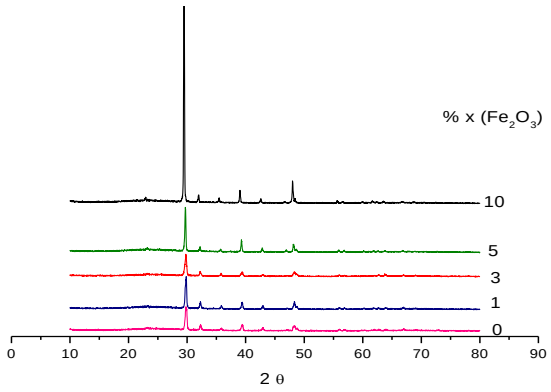

DRX patterns of as-prepared SG iron containing samples

Based on the information obtained from X-ray diffractograms regarging the presence of residual nitrates, it was decided to wash the samples in distilled water for 1h and 30 min, after which they were filtered through 100 micron filters. After washing and heat treatment at 600 ^oC, X-ray diffraction analysis shows that the nitrates crystalline phase dissolved during the wash. Moreover, for samples with high iron concentration, it is emphasized that after treatment they have a non-crystalline structure, while for samples with a lower iron concentration a new

crystalline phase is developed, as evidenced by the lines recorded in the range $20 \leq 20 \leq 36^{o}$ which are specific to silicon oxide in the form of cristobalite.

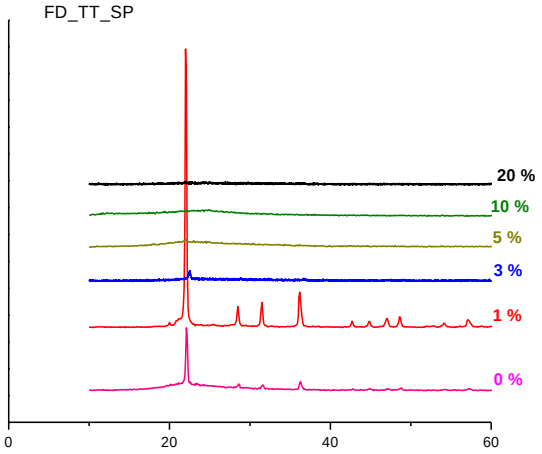

DRX patterns of heat-treated FD iron containing samples

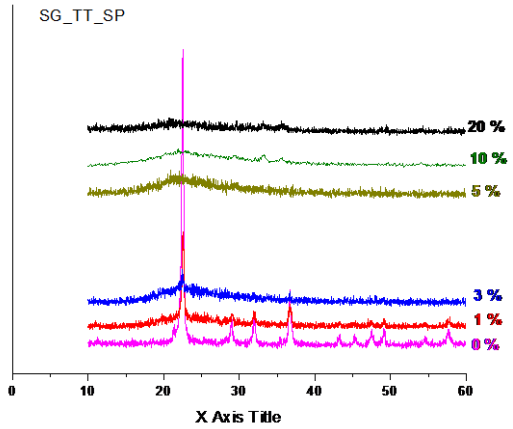

DRX patterns of heat-treated SG iron containing samples

These structural differences between samples with up to 3% Fe_2O_3 and those with higher iron content are also observed by infrared spectroscopic analysis of thermally treated samples.

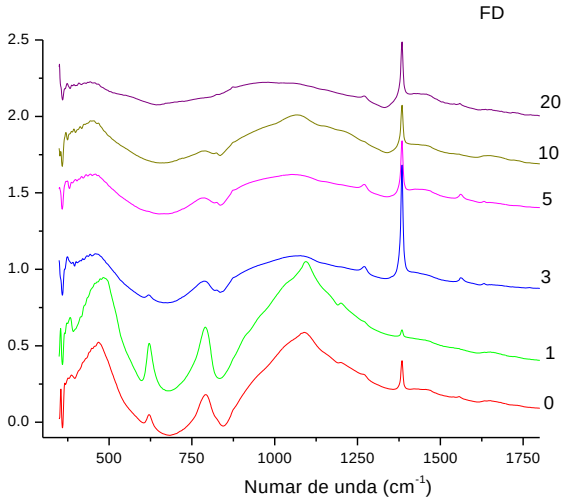

FT-IR spectra of heat-treated FD samples

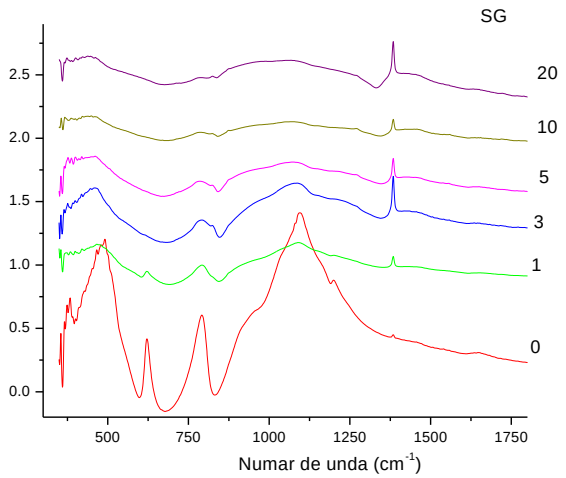

FT-IR spectra of heat-treated SG samples

In-vitro bioactivity test was done after samples immersion in simulated body fluid (SBF) for a period of 14 days.

Atomic concentrations at the sample surface were determined from the XPS survey spectra. Samples were analyzed both before and after 14 days incubation in SBF at 37 °C under static conditions. The chemical composition on the outermost layer, determined by XPS, and that determined by EDXS in a deeper layer, was investigated both before and after 14 days of immersion in the SBF for the 3 and 5% samples which proved to be biocompatible with tested cellular medium.

Elemental composition (at %) determined by XPS analysis before and after immersion in SBF

Elements → Sample↓		C	O	Si	Na	Fe	N	Ca	P
x=3	Before immersion in SBF	19.8	48.1	19.2	10.9	0.6	1.4	-	-
	After SBF immersion	11.0	50.5	30.0	2.6	0.4	1.3	2.9	1.3
x=5	Before immersion in SBF	19.6	46.5	23.0	9.2	0.8	0.9	-	-
	After SBF immersion	19.1	46.8	28.2	2.6	0.5	0.7	1.6	0.5

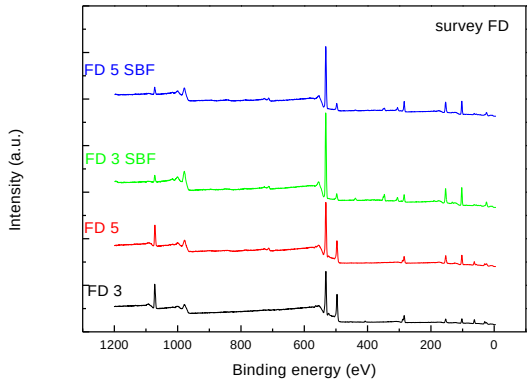

XPS survey spectra for FD samples

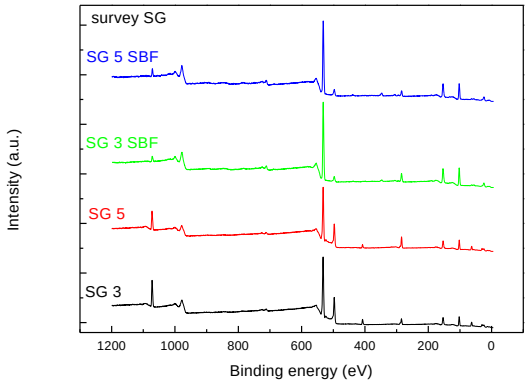

XPS survey spectra for SG samples

Regarding the iron ions, the results obtained by EPR spectroscopy yields details on the sites occupied by Fe^{3+} ions in the sodium-silica host matrix. The EPR spectra mainly consist of two resonance lines at $g_{eff} \approx 4.3$ and 2.0. The $g_{eff} \approx 4.3$ component is assigned to isolated Fe^{3+} ions in sites of low symmetry characterized by high crystal fields and that at $g_{eff} \approx 2.0$ to Fe^{3+} ions in sites of octahedral symmetry, with low crystal fields and to iron ions that are experiencing strong dipolar and/or superexchange interactions. The intensity of $g_{eff} \approx 2.0$ line increases while that of $g_{eff} \approx 4.3$ line decreases with Fe_2O_3 content and for $x \geq 10$ mol% Fe_2O_3 is barely noticeable. For the sample with x = 5 mol% Fe_2O_3 an additional narrow line is observed beside the large $g_{eff} \approx 2.0$ line, with the width about 100 G and could be related to a superparamagnetic phase of iron oxide, and this composition was considered of interest for further investigations as potential MRI contrast agent and hyperthermia vector.

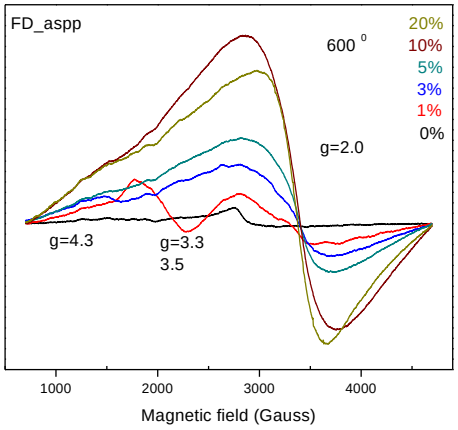

Fe^{3+} EPR spectra of as-prepared FD samples

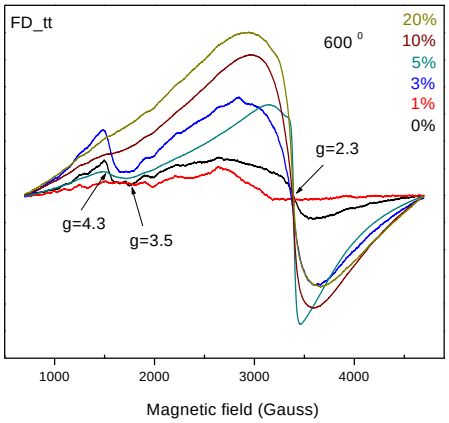

Fe^{3+} EPR spectra of heat-treated FD samples

^{29}Si MAS-NMR spectra of the as-prepared samples indicate a polymerization of the silicate network (with a shift of the ^{29}Si MAS-NMR spectrum center to higher chemical shift values) as well as a short- and medium-range disorder effect noticed by decrease of Q_2 and Q_3 units in favor of the Q_4 units, when higher iron content is introduced in the silicate network. In such cases, the deconvolution of ^{29}Si NMR spectra is not unique.

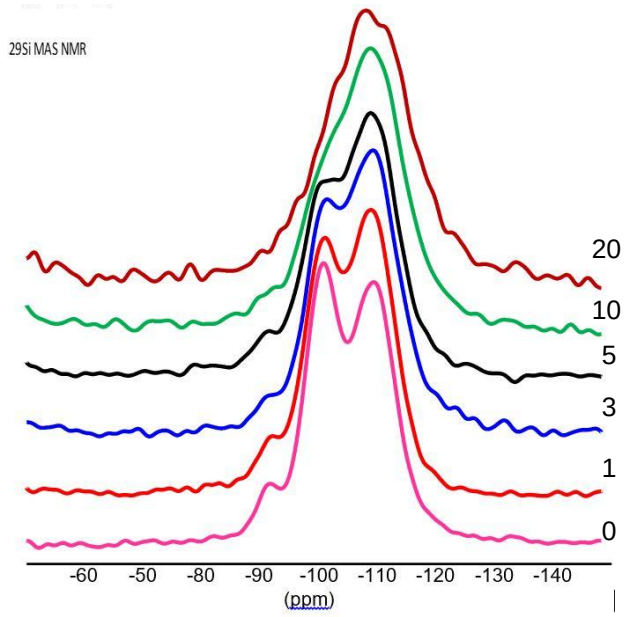

^{29} Si MAS NMR spectra of as-prepared FD samples

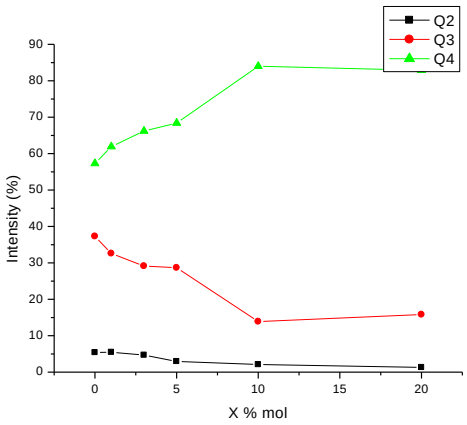

Fraction of Q^n units in as-prepared FD samples

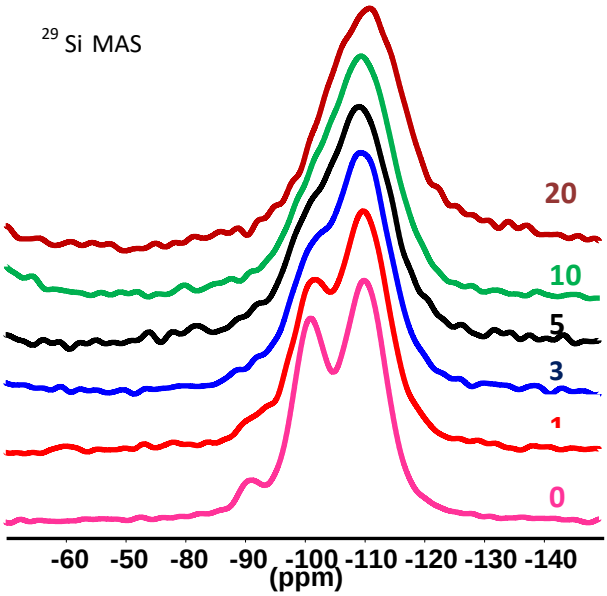

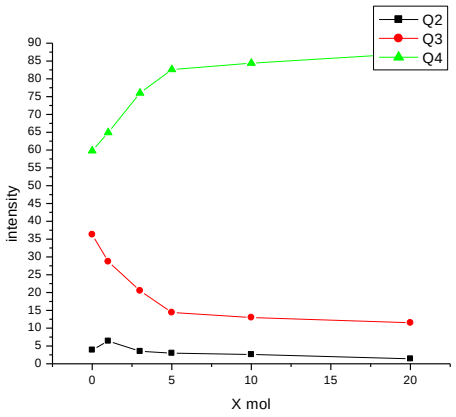

[29] Si MAS NMR spectra of as-prepared SG samples

Fraction of Q^n units in as-prepared SG samples

As can be seen from MRI images *in vitro*, the iron samples behave as contrast agent by T_2, also confirmed by computation data obtained using MRI relaxometry protocol. For the quantitative verification, the relaxometry analysis with the RARE-T_1 + T_2-map protocol was performed, allowing the evaluation of T_1 and T_2 relaxation times.

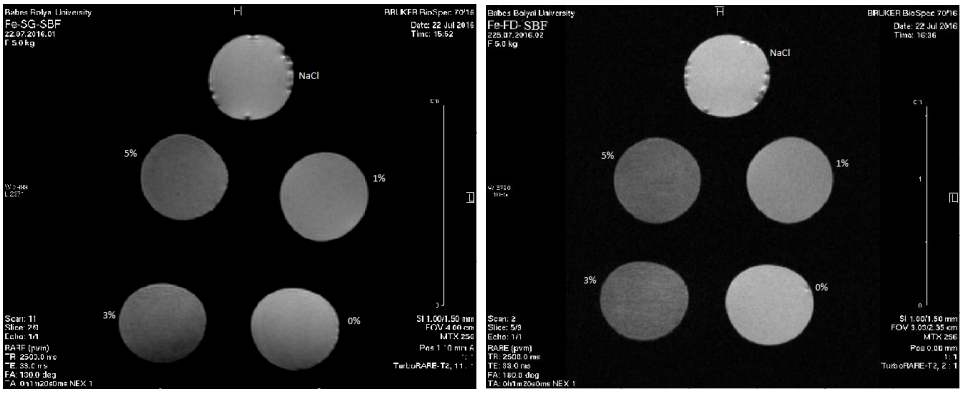

T_2-weighted images for FD samples acquired using Turbo RARE protocol for (a) SG and (b) FD samples after immersion in SBF

The relaxometry curves were obtained from the images acquired with the protocol dedicated to transverse relaxation, Turbo Rare T_2. As can be observed in the above images, the contrast increases with increasing iron addition, and in both cases the 5% Fe_2O_3 concentration provides the best contrast.

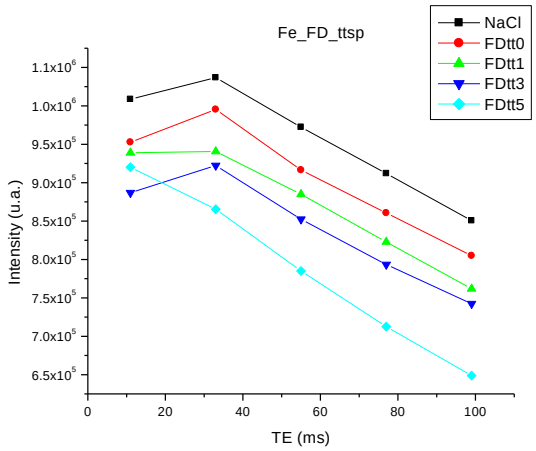

MRI signal intensity, in a.u., measured at different echo times, for FD samples

As with FD samples, for SG samples it was also confirmed that with the increase in paramagnetic ions concentration, the samples behave as a negative contrast agent, i.e. decreases the relaxation time T_2 of the entire system in which it has been diluted.

The studies were supplemented with tests to check a possible cytotoxic effect induced by these compounds by monitoring the control cells and cells treated with different concentrations of SG and FD samples using the phase contrast optical microscope. This allowed immediate identification of cell morphology and comparison of control cells with treated cells with different concentrations of SG and FD samples. Both MTT, the real-time proliferation assay using MTT 3- (4,5-dimethylthiazol-2-yl) -2,5-diphenyltetrazolium and the „wound healing" technique led to the following conclusions:

- a concentration higher than 5% of either SG or FD samples affect cell viability and proliferation; moreover, these concentrations of substance lead to cell death;

- of all concentrations tested, 1%, 3%, 5% and related dilutions allowed to obtain relevant data suggesting applicability both *in vitro* and *in vivo*;

- the optimal 5% concentration did not have a toxic effect on the cell lines chosen for this study, nor was morphology, proliferation, migration and repair ability of the injured area and cell adhesion affected. Following biocompatibility tests, which showed that samples with higher concentration, i.e. 10% and 20% Fe_2O_3, destroyed the cells completely, it was decided to remove them from subsequent studies, keeping only the samples that passed the biocompatibility test.

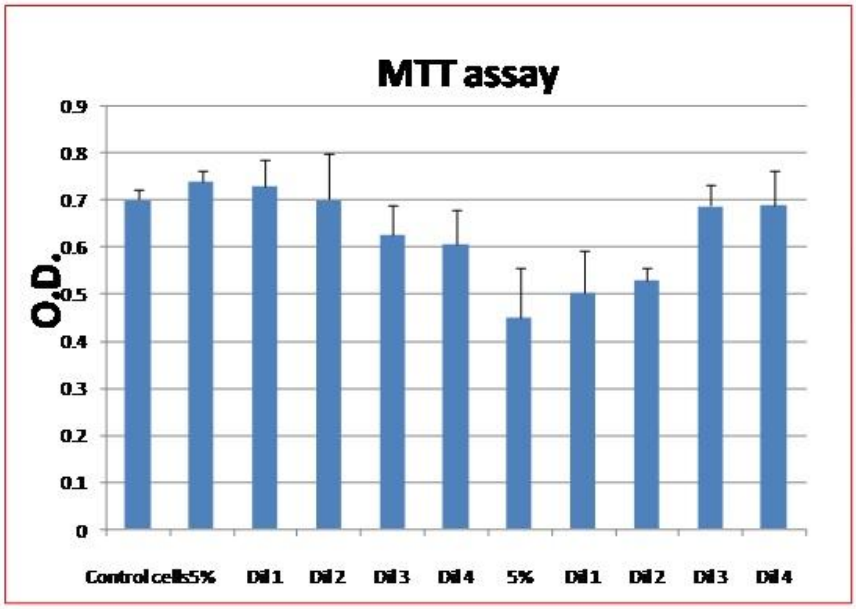

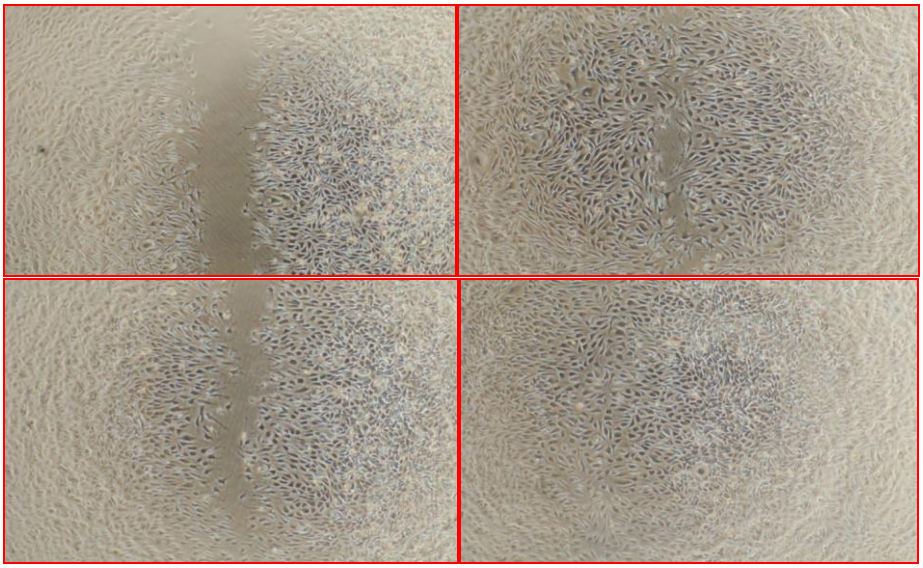

The cytotoxicity test,using MTT (top) and "wound healing" technique (bottom)

After examining the biocompatibility and relaxometry results, the samples of choosen compositions were tested *in vivo* as contrast agents for MRI, selecting for rat injection the 3% and 5% samples obtained by the two methods immersed in SBF. The experimental model was developed in accordance with the guidelines on accommodation and care of animals drawn up by the European Convention for the protection of vertebrate animals used for experimental and other scientific purposes.

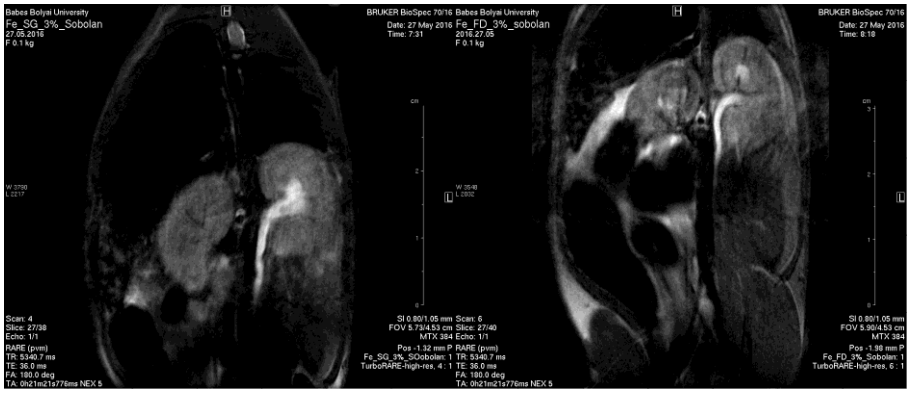

Morphological MRI investigation to assess the contrast characteristics of 3% iron compounds. Sodium chloride with SG (left) and FD (right) samples were injected.

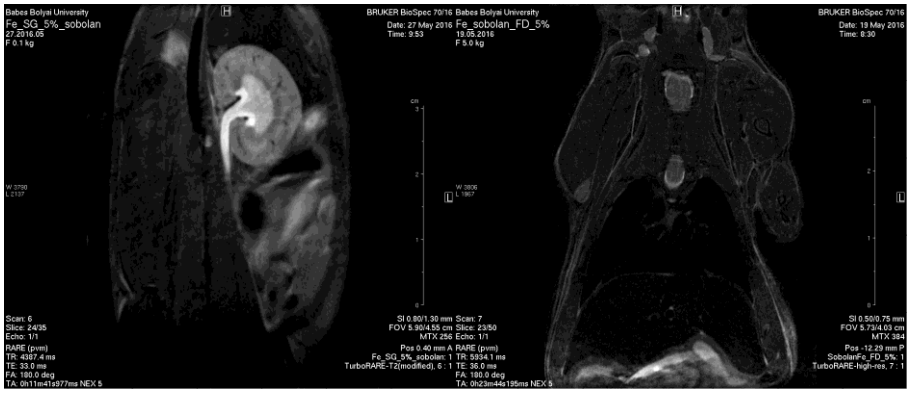

Morphological MRI investigation to assess the contrast characteristics of 5% iron compounds. Sodium chloride with SG (left) and FD (right) samples were injected.

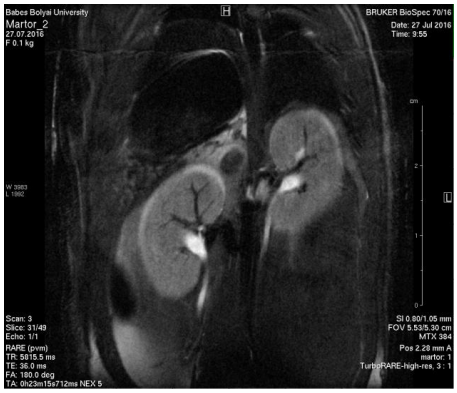

Morphological MRI investigation of a control rat

The images are recorded for rats injected with dilute solution with 3% and 5% concentration for the two synthesis methods, compared to an image representing a control rat. Good contrast is obtained for the injected rats and the contrast substance obtained is carried through the blood throughout the tissue. MRI acquisitions were performed with the TurboRARE-high-res protocol dedicated to T_2 relaxation imaging and the TurboRARE-T_2 protocol.

Final histopathology tests showed low hepatic toxicity but no iron deposition in the hepatocytes was observed. Examination of renal fragments did not reveal any notable histopathological changes.

Conclusions

on Dy_2O_3 containing system

Microparticles (100-x) $SiO_2 \cdot xDy_2O_3$ ($0 \leq x \leq 10$ mol%) with 1-4 μm sizes were obtained by three sol-gel synthesis methods: classical sol-gel (SG), lyophilization (FD) and spray-drying (SD), thereafter heat treated at 600 ° C, based on DTA / TGA analysis results.

The ^{29}Si MAS-NMR results indicate for the samples obtained by FD method a greater interconnectivity of the structural units than for the samples obtained by the SD method and an increased polymerization of the silicate network with the addition of dysprosium oxide.

The XPS surface analysis shows that dysprosium appears on the outermost layer of these particles in a concentration close to the theoretical value, but for the sample with 10 mol% Dy_2O_3 a partial agglomeration of dysprosium on the microparticles surface is shown. The higher NBO/BO ratio on the surface of the samples with 5% than on those with 10% Dy_2O_3 supports the hypothesis of partial agglomeration of dysprosium that breaks the silicate network.

The MRI contrast agent properties tested with the RARE-T1 and Rare-T2 protocols indicate that the dysprosium containinf samples have negative contrast agent characteristics. The relaxometry curves show that the best contrast is given by the sample with a 5 mol% Dy_2O_3 obtained by FD method, which, as shown by the *in vitro* tests, provides an increased number of dysprosium ions on the surface of the microparticles due to high surface/volume ratio and the advanced depolymerization in the silica host matrix.

From the point of view of biocompatibility performed on HUVEC cells, umbilical cord specific cells, the biocompatible samples obtained by the three methods of preparation can be used for *in vivo* tests. All the more, the tests performed on DLD1 carcinogenic colon cancer cells show that the same samples and their dilutions, which are biocompatible with HUVEC cells, largely destroy the carcinogenic cells of the DLD1 type.

on Fe_2O_3 containing system

Micrometric particles of $(100\text{-}x)[0.5SiO_2 \cdot 0.3Na_2O] \cdot xFe_2O_3$ ($0 \leq x \leq 20$ mol%) composition were obtained by the classical sol-gel method and freeze-driying, and subsequently they were heat treated at 600 °C. This iron containing system could also be considered for applications in hyperthermia treatments.

Using the ^{29}Si MAS-NMR analysis method, it was emphasized that the iron oxide addition to sodium-silicate matrix and the thermal treatment resulted in a slight depolymerization of the network for the thermally treated samples.

Electron spin resonance lines centered around $g \approx 4.3$ and $g \approx 2.0$ are influenced by increasimg iron concentration and heat treatment, reflecting the fact that in the iron-rich regions the Fe^{3+} ions are not homogeneously distributed.

Depending on drying method of samples, the scanning electron microscopy images show different morphologies. After immersion in SBF, the samples obtained by both methods have a small grain size and a porous structure with pore sizes between 30-65 nm for samples immersed in SBF.

The decrease in iron content on samples after immersion in SBF, evidenced by the XPS analysis, is due to calcium and phosphorus samples that migrate from the SBF on samples surface.

The relaxometry data show that 1, 3 and 5 mol% Fe_2O_3 samples have a T_2 relaxation time lower than that obtained for the NaCl solution or for the iron free sample. MRI images for *in vitro* tests reveal a better contrast for samples with 5 mol% Fe_2O_3.

Biocompatibility tests show that 1, 3 and 5 mol% Fe_2O_3 samples do not cause major changes on the cells, and are therefore recommended for animal model in vivo tests.

Selective references

[1] M. Mocan, **L. Chiriac**, O. Banc, R. Moldovan, F. Turcu, and S. Simon, Magnetic resonance imaging based assessment of aortic valve area: A methodology proposal and an experimental case study, *Hum. Vet. Med.* 2015, 7 (4) 327–333.

[2] A. Staicu, R. Popa-Stanila, **L. Chiriac**, D. Gheban, G. Caracostea, F. Turcu, S. Simon, F. Stamatian, Rare renal anomalies described in second trimester foetuses using post mortem MRI case series, *Obstr. Ginecol.* 2015, 63 (3).

[3] A. Staicu, R. Popa-Stanila, D. Gheban, **L. Chiriac**, F.R.V. Turcu, G. Caracostea, F. Stamatian,Imagistic and histopathological description of a cystic nephroma during early second trimester of gestation, *Med. Ultrason.* 2017, 19 (3) 327-329.

[4] E. Horvath, A. Hutanu, **L. Chiriac**, M. Dobreanu, A. Oradan, E.-E. Nagy, Ischemic damage and early inflammatory infiltration are different in the core and penumbra lesions of rat brain after transient focal cerebral ischemia, *J. Neuroimmunol*. 2018, 324, 35-42.

[5] A. Hutanu, E. Horvath, A. Oradan, S. Voidazan, **Chiriac**, D.L. Muntean, M. Dobreanu, Fish-oil preconditioning modulates plasma MCP-1 and TIMP-1 levels after experimental induced transient cerebral ischemia, *Farmacia* 2018, 66 (4) 602-608.

[6] P. Prabhu, V. Patravale, The upcoming field of theranostic nanomedicine: An o overview, *J. Biomed. Nanotechnol.*, vol. 8, no. 6, pp. 859–882, 2012.

[7] E. Terreno, F. Uggeri, S. Aime, Image guided therapy: The advent of theranostic agents, *J. Control. Release*, 2012, 161 (2) 328–337.

[8] M.A. Busquets, J. Estelrich, M.J. Sanchez-Martin, Nanoparticles in magnetic resonance imaging: from simple to dual contrast agents, *Int. J. Nanomedicine*, 2015, 140 (10) 1727-1741.

[9] R.A. Assink, B.D. Kay, Sol-gel kinetics III. Test of the statistical reaction model, *J. Non-Cryst. Solids* 1988, 107 (1), 35-40.

[10] L.L. Hench, J. K. West, The Sol-Gel Process, *Chem. Rev.* 1990, 90 (1) 33–72.

[11] **L.B. Chiriac**, D.L. Trandafir, R.V.F. Turcu, M. Todea, S. Simon, Synthesis, structural characterization and in vitro testing of dysprosium containing particles as potential MRI contrast enhancing agents, *Appl. Surf. Sci*. 2016, 385, 569-577.

[12] **L.B. Chiriac**, M. Todea, A. Vulpoi, M. Muresan-Pop, R.V.F. Turcu, S. Simon, Freeze-drying assisted sol–gel-derived silica-based particles embedding iron: synthesis and characterization, *J. Sol-Gel Sci. Technol*. 2018, 87 (1) 195-203.